Characterization of an Aeroacoustic Wind Tunnel Facility

Kyle PASCIONI[1]; Robert REGER[2]; Adam EDSTRAND[3]; Louis CATTAFESTA[4]

Florida Center for Advanced-Aero Propulsion (FCAAP)

Florida State University, USA

ABSTRACT

The Florida State Aeroacoustic Tunnel (FSAT) is an open-circuit anechoic wind tunnel designed for low subsonic aerodynamic noise studies. Nominal flow speeds in the test section range from 5-75 m/s and are achieved using a 450-hp centrifugal blower. The test section, with dimensions $0.914\times 1.219\times 3.048$ m (H×W×L), can take the form of an open-jet or closed-wall configuration. A 250 Hz anechoic chamber ($2.7\times 4.5\times 4.8$ m) surrounds the test section. Flow non-uniformity and turbulence intensity are measured to be <1% and <0.12%, respectively, for both test section configurations at all flow speeds. To enhance acoustic quality, an inlet silencer is placed upstream at the entrance of the tunnel, while a metal perforate liner is used over the entire length of the diffuser. Additionally, a swiveling jet collector rotates ±10 degrees for lifting bodies that deflect the freestream jet. Depending on frequency, background noise levels are found to scale with Mach number between the fifth and eighth power, and are 80 dBA at Mach 0.17. The major noise sources are determined to be the first set of turning vanes, jet collector, and the fan/motor. Reduction techniques of these noise sources are proposed and will be considered in future work.

Keywords: Aeroacoustics, Anechoic Wind Tunnel, Airframe Noise
I-INCE Classification of Subjects Number(s): 51.4

1. INTRODUCTION

Global projections are expecting the passenger aircraft fleet to double by 2032 [1]. With this increase in air traffic, it is necessary to address the effect of noise pollution on communities adjacent to airports. It is well known ultra–high bypass engines and other low–noise propulsive technologies have greatly reduced the overall noise levels in the last few decades. However, further reduction is necessary at approach conditions, where the airframe is the dominant noise source in certain configurations [2]. Flow unsteadiness is generated over complex geometries and propagates as sound to the far field. Components such as high-lift devices (leading edge slats, flap side-edge, trailing edge, etc.) and deployed landing gear systems produce high levels of turbulence and can also have flow-acoustic resonant characteristics. The facility at Florida State University (FSU) which is characterized herein is aimed at understanding aerodynamic sound sources generated by these various airframe components. Knowledge of the governing flow physics will not only enhance prediction tools for low-noise aircraft design, but also provide guidance for reduction techniques (e.g., using flow control) which typically entail large parametric studies.

This wind tunnel has been designed similar to conventional tunnels used in aerodynamic research but is modified with extended capabilities to allow aeroacoustics to be studied. The goal is to provide a test environment that mimics a radiative free field capable of generating high-quality fluid dynamic and acoustic measurements. Sub-component scaled tests are studied similar to the experiments conducted in this facilities' predecessor [3, 4]. Two key design metrics include a maximum freestream Mach number of 0.2, enveloping typical approach conditions, and tunnel background noise at least 10 dB lower [5] than typical sound pressure levels produced by the physical model under test.

This work focuses on characterizing the flow and acoustic quality of the Florida State Aeroacoustic

---

[1]kpascioni@fsu.edu
[2]rreger@fsu.edu
[3]aedstrand@fsu.edu
[4]lcattafesta@fsu.edu

Tunnel (FSAT). An overview of the facility is first given. Measurements of the jet quality (velocity profiles and turbulence intensity) are then analyzed. An acoustic characterization of the anechoic chamber (no flow) and background noise levels (with flow) are also presented, followed by a brief summary of expected acoustic upgrades.

2. FACILITY OVERVIEW

The Florida State Aeroacoustic Tunnel (FSAT) is an open-circuit, open-jet anechoic wind tunnel designed for subsonic aerodynamic and aeroacoustic studies. The first section describes the general facility layout. The next two sections give additional details of the anechoic chamber and modular closed-wall test section.

2.1 Summary of Tunnel Components

FSAT, as shown in Figure 1, is driven using a downstream centrifugal blower powered by a three-phase 450 hp (900 rpm) motor. Outside air is pulled through the 3.66×2.44 m inlet equipped with a symmetric vaned silencer. This silencer is composed of six vertical vanes lined with perforate metal to occlude outside ambient noise. A honeycomb section and six conditioning screens are then met for flow straightening and turbulence reduction, respectively. The screens are stainless steel wire mesh and decrease in mesh size from 9 to 22 wires per centimeter. The aluminum honeycomb section consists of 1 cm hexagonal cells installed between the first and second screen. The flow then passes through a settling chamber outfitted with 45 ports to allow seed injection for non-intrusive fluid dynamic measurements (e.g., particle image velocimetry, laser Doppler velocimetry). An 8:1 area contraction is contoured using fiberglass laminate and designed to accelerate the flow to the test section speed without separation. The air is then expelled in the 0.914×1.219×3.048 m (H×W×L) open-jet test section enclosed by an air-tight 250 Hz anechoic chamber. The center of the chamber is offset in the tunnel spanwise direction (north to south per Fig. 1) to allow greater far field measurement distances, up to 2.3 m. Also, the model test stand is designed so the majority of the structure is upstream of the test section to minimize acoustic reflections.

The flow enters the jet collector upon exiting the test section. The jet collector is designed to be large enough to minimize jet impingement, but small enough to restrict divergence of the potential core. To accomodate lifting bodies in an open-jet configuration, the collector is designed to swivel ±10° off the streamwise axis in an effort to avoid higher background levels and flow recirculation in the chamber. 2.26 m downstream of the collector is the first set of 90° turning vanes. Each vane is a hollow aluminum extrusion filled with sand for vibration damping. The flow travels approximately 10 m through a diffuser progressively increasing in area. Another set of 90° turning vanes passes the flow outside of the building to the aforementioned fan/motor system. The full length between the jet collector and fan is lined with perforate metal to attenuate both flow and fan noise propagating upstream. To minimize structural acoustic contamination, the fan and motor are isolated from the diffuser using a 10 cm deformable coupling and mounted on a large isolated concrete slab. Rubber pads are also placed between all ducting components and their respective frame.

Programmable speed is accomplished through a variable frequency drive (Danfoss Model FC-302) connected to a National Instruments cDAQ-9174 subject to a linear relationship between input voltage and fan frequency. Freestream conditions (static pressure and temperature, dynamic pressure, and relative humidity) in the test section are monitored and recorded using LabView software. Reynolds number is found to have a standard deviation of <0.15% of its mean value for all flow speeds over 10 m/s.

2.2 Anechoic Chamber

The anechoic chamber is 2.7×4.5×4.8 m (H×W×L) wedge–tip to wedge–tip. The cloth–covered fiberglass wedges are mounted to the vertical cinderblock walls and ceiling in an alternating pattern for improved acoustic absorption. The wedge–tip to valley length (34.3 cm) is approximately 1/4 wavelength of a 250 Hz acoustic wave at standard temperature and pressure, defining the nominal chamber cutoff frequency. The wedges are offset approximately 25 mm from each wall to further assist in low frequency damping. Wedges are also placed on the floor to create a fully anechoic environment. The entire chamber is air–tight when the doors to the chamber are closed. The outer surfaces of the tunnel components protruding into the chamber (contraction and jet collector) and the model test stand are treated using foam wedge sheets.
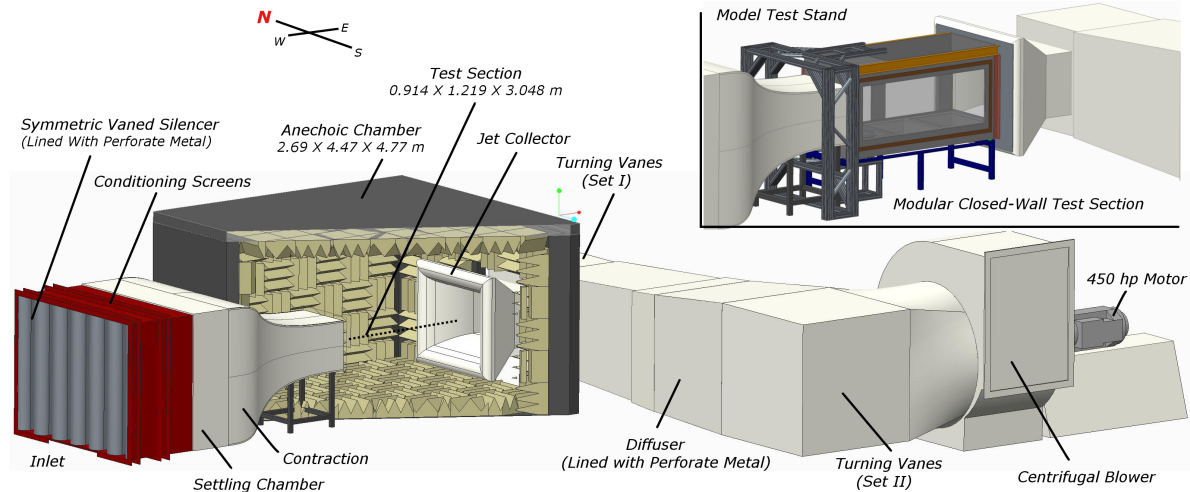
Figure 1 – Schematic of the Florida State Aeroacoustic Tunnel showing both the open-jet configuration and the closed-wall test section installed (top right). Flow direction is left to right, and the anechoic chamber is cut for illustration.

2.3   Modular Closed-Wall Test Section

It is well known that an open-jet alters the aerodynamics of lifting models. This is due to the difference in boundary conditions, i.e., the lack of an "infinite" freestream found in actual flight. Thus, lifting bodies often require a larger geometric angle of attack to match mean pressure distributions and/or overall lift. For low blockage models, a closed-wall test section allows a closer match of the infinite freestream case. Therefore, this facility is equipped with a modular closed-wall test section yielding flow characteristics similar to a conventional wind tunnel. This capability extension is beneficial for source localization since the near field hydrodynamics are coupled with the energy being radiated to the far field; the disadvantage being in a reverberant environment.

The closed-wall test section has identical dimensions as the open-jet test section. It is framed in black anodized aluminum with a combination of acrylic and glass panels to maximize optical access. When installed, it is bolted directly to the end of the contraction. The junction between the test section and jet collector is capable of a smooth sealed transition if desired.

3.   FLOW FIELD CHARACTERIZATION

This section discusses the metrics used to quantify the quality of the freestream flow. Velocity profiles illustrate the breakdown of the jet potential core, while hot-wire anemometry captures turbulence properties of the open-jet and closed-wall test sections.

3.1   Flow Non-Uniformity

The extent of the potential core is an important aspect of aeroacoustic measurements. Not only does the shear layer generate self-noise and refract noise generated by the model, its impingement on an aerodynamic surface can cause high levels of noise that can corrupt far field acoustic measurements. Therefore, the extent of the potential core must be quantified to determine proper streamwise placement of the model under study.

Velocity profiles are measured using a 32-port Pitot rake with 2.54 cm spacing. Two 16-channel pressure scanners (Scanivalve DSA3217 1 psid modules) acquire each port at 2 Hz. Stagnation pressure of the rake ports are measured relative to the static port of a Pitot-static probe mounted upstream at the beginning of the test section. Three streamwise stations are measured, $x/L = 0.04, 0.5, 0.85$, where L is the test section length. The rake is oriented horizontally (parallel to the ground) and vertically (perpendicular to the ground) to map out the flow profiles along the respective test section lengths, b and h. Denoting the mean freestream speed as U_∞, data are acquired at several speeds, but only $U_\infty = 36$ m/s is given in Fig. 2 for brevity. Measurement uncertainty is found to be $\pm 2.2\%$ of U_∞ in the core. The reduction of the vertical and horizontal extent of the potential core as the jet progresses downstream is clearly seen, and is reduced by 30% at $x/L = 0.85$. Less than 1% non-uniformity is found for all positions in their respective core regions.
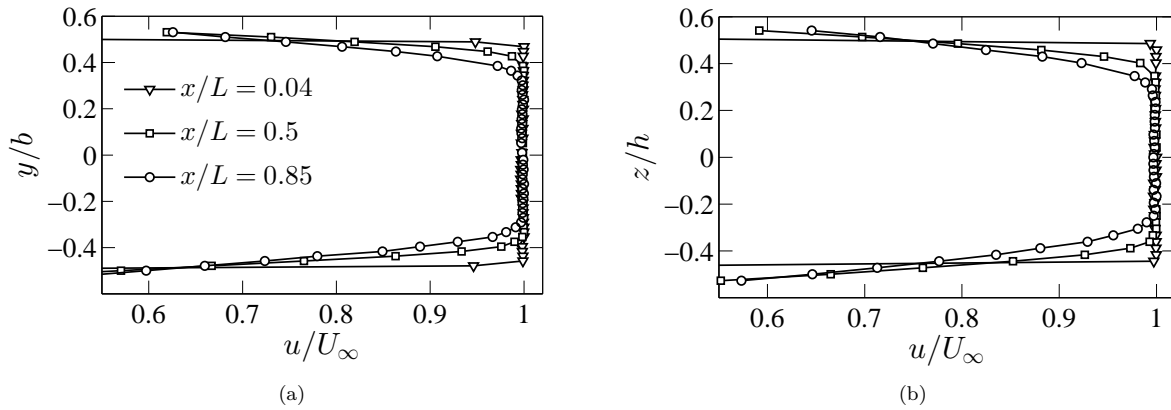
(a)

(b)

Figure 2 – Velocity profiles acquired using a Pitot rake at various streamwise stations. $U_\infty = 36$ m/s for (a) horizontal and (b) vertical directions, where b and h are the horizontal and vertical test section dimensions, respectively.

3.2   Freestream Turbulence

The assessment of freestream turbulence is also a necessity for characterizing any new aerodynamic facility. If the freestream turbulent fluctuations are too great, both the flow physics and aeroacoustics can be affected. Constant temperature hot-wire anemometry is used to quantify the freestream turbulence intensity, which is defined as the ratio between the root-mean-square of the velocity fluctuations and the mean velocity,

$$TI = u'_{rms}/U_\infty. \tag{1}$$

Levels are deemed acceptable if they are low enough as to not significantly affect the critical Reynolds number for transition. This standard turbulence intensity is approximately <0.1% since this is shown by Schlicting [6, chap. 16] to have little effect on the transitional Reynolds number of a laminar flat plate boundary layer at zero incidence. The hotwire time signal is digitized using a National Instruments PXI-1045 chassis with a PXI-4462 DAQ card. Sampling frequency is set to 8,192 Hz which is within the limiting bandwidth of the Dantec Streamline system using a CTA 90C10 Module. A single sensor wire probe 5 μm in diameter and 1.5 mm in length is used for all cases. Calibration is performed by a Dantec 90H02 Flow Unit using King's Law, with the exponent of the power fit nominally 0.4. The probe is mounted on a NACA0012 airfoil effectively decreasing the bluff body shape of the mount to minimize probe vibrations which are known to corrupt the signal. Since a single sensor probe can only output a one dimensional measurement, data are acquired with the probe in both a horizontal and vertical orientation, for vertical and lateral fluctuations, respectively. Additionally, the probe is traversed to multiple positions in the test section to ensure turbulence homogeneity. Very little deviation is found between probe orientation as well as location, hence, for this discussion turbulence isotropy and homogeneity will be assumed. Therefore, sample data provided in this section are at the test section center with a horizontal probe.

Figure 3(a) gives the velocity spectra of the fluctuations for three tunnel speeds. The autospectral random uncertainty is found to be 2.58%. Broadband levels tend to increase with tunnel speed and are slightly higher for the open-jet case. The only significant narrow-band peaks are present in the 35 m/s case, but are not thought to be produced by the flow. Identical peaks are found in the noise floor; hence, these features are likely electronic noise in the voltage signal.

Low frequency oscillations are considered to be bulk flow unsteadiness as opposed to turbulence. It can be argued, by Bradshaw's [7] definition, any phenomenon with a characteristic length scale greater than the largest dimension of the test section is not turbulence. This large scale bulk movement can be due to slight variations in the fan frequency, deviations in ambient conditions, or possibly a jet column mode [8] created by the interaction of the shear layer with the jet collector. It is for this reason the raw time signal is post processed with a fourth-order Butterworth high-pass filter. The 3–dB cutoff frequency of the filter is determined using the largest test section dimension by the relation

$$f_{3dB} = U_\infty/(2L), \tag{2}$$

and varies from 1–11 Hz. Figure 3(b) provides the high-pass filtered turbulence intensity for a large range of tunnel speeds. At first glance, the highest turbulence levels are found to be below 25 m/s.
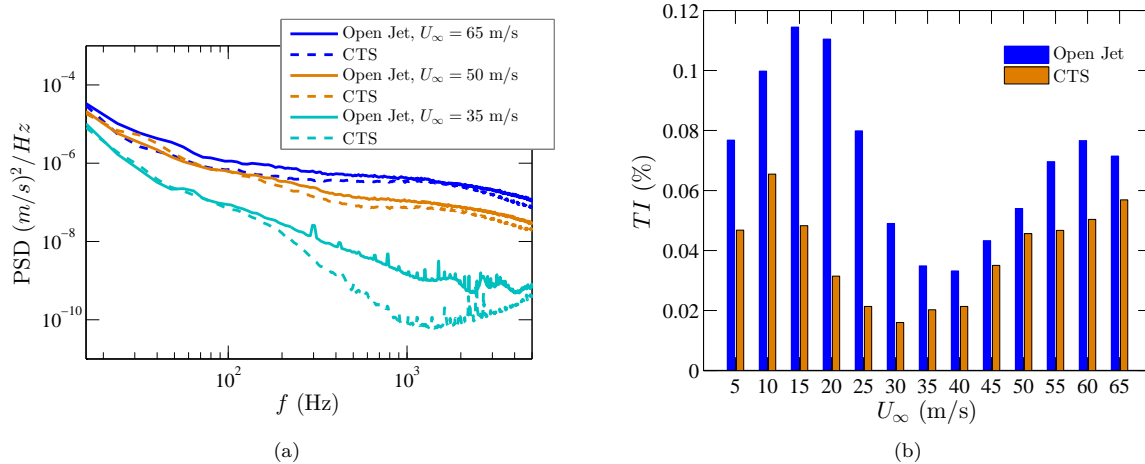
(a)

(b)

Figure 3 – Freestream turbulence metrics, where (a) is the velocity spectra and (b) is the high-pass filtered turbulence intensity of the empty test section for the open-jet and closed-wall test section (CTS) configurations.

However, as the low frequency fluctuations carry the majority of energy, the levels shown here are very sensitive to f_{3dB}. Lower tunnel speeds decrease f_{3dB}, and hence, can greatly influence the turbulence intensity calculation (Equation 1). In any case, the levels are competitive for both tunnel configurations and lower than 0.12% for all flow speeds.

4.   ACOUSTIC CHARACTERIZATION

Acoustic measurements are completed with and without flow. The no-flow case will first be discussed and focuses on the anechoic chamber's ability to synthesize a free field environment. The flow case will then be presented to provide baseline measurements of the background noise. Suggestions for improving the acoustic quality will follow. For consistency, the acoustic reference pressure used throughout this section to calculate dB levels is 20 μPa.

4.1   Free Field Quality

Certification of the anechoic chamber is performed using the ISO 3745-2003 standard, Annex A [9]. Pink noise is generated from an audio source just above the floor wedges and centered in the chamber. Measurements are obtained using a traversing 1/2" free field microphone (Brüel & Kjær 4189). Five linear traverses are set, four into the trihedral corners, and the remaining traverse mapping out the vertical coordinate directly above the speaker.

Figure 4 provides the acoustic pressure decay with distance from the source at selected 1/3 octave bands along each traverse. The corner directions correspond to the compass defined in Fig. 1. Allowable deviations from the inverse-square-law [9] are also plotted to illustrate the free field quality. 6–dB per doubling of distance, which is realized by an acoustic wave in a non-reflective environment, is also characteristic of this anechoic chamber. The largest divergence is in the southwest corner traverse due to the close proximity of both the contraction exit and the model test stand. However, this slight deviation is found to be permissible as the bulk of measurements occur on the north wall. The trends found in the lowest frequency band confirm the chamber to be anechoic down to 250 Hz.

4.2   Background Noise

The background noise determines the nominal effective noise floor at a given tunnel speed. The test section is in the open-jet configuration (no closed-wall test section) and without sidewalls, as depicted in Figure 1, but with the test stand installed and acoustically treated. The two dominant types of noise are flow-induced and those which are mechanically generated (i.e., the fan/motor system). To measure this noise floor, a linear array of six free field microphones (1/4" G.R.A.S. 40BE) are positioned sideline 1.6 m from the test section center (ground parallel toward the north wall), and level with the vertical center of the test section. A–weighted overall sound pressure level (OASPL(A)) can be found in Fig. 5(a) from the microphone 0.71 m downstream of the contraction exit. Spectra of the array microphones are nearly identical in amplitudes as well as frequency content. A–weighting is applied to both metrics to inhibit low frequency dominance, as the majority of the
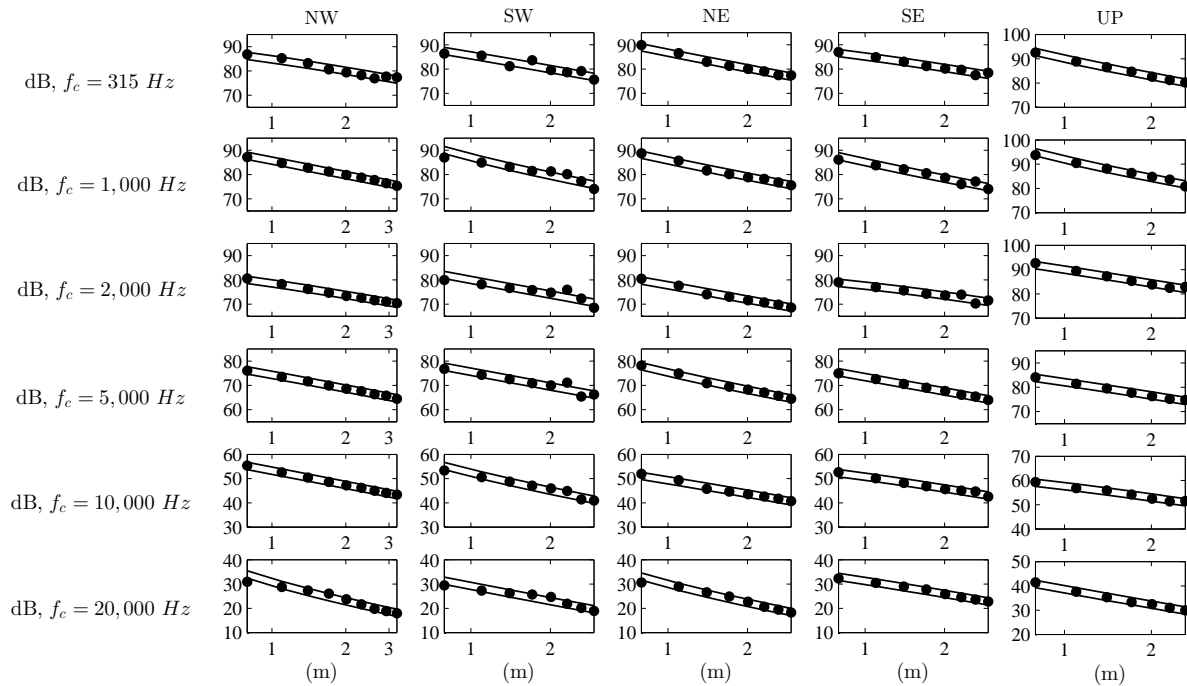
Figure 4 – Selected 1/3 octave bands illustrating acoustic decay with distance from the audio source to the four trihedral corners and vertical direction, as defined by the compass in Fig. 1. f_c is the center frequency of each band, and allowable deviation [9] are plotted as solid lines.

aerodynamic models with length scales appropriate for the FSAT test section peak beyond 1 kHz. It should be noted OASPL is found by integrating the A–weighted spectrum from the chamber cutoff frequency to 20 kHz. The upper integration limit is arbitrary as 99% of the energy is contained in frequencies less than 1 kHz. Ease of installation set the ground parallel location; however, typical measurement stations are often further from the jet, and is the reason all plots are scaled to 2.3 m using the geometric spreading relation. It was found early on that although the jet collector surface is metal perforate, ideal for grazing flow, shear layer impingement noise is dominant. This realization motivated additional treatment to be installed, and took the form of 3.8 cm thick Nomex® to blanket the surface. OASPL(A) is reduced by at least 2 dB across the complete tunnel speed range. Fig. 5(b) is the A–weighted 1/3 octave band SPL with the newly treated collector face. Peak values are around 600–700 Hz. As the tunnel speed is increased, the amplitude of each frequency band is also uniformly increased. This suggests the dominant sources holding specific frequency content are always dominant, independent of flow speed.

The SPL plots in Fig. 5(b) can be scaled to elucidate the Mach number dependence. This scaling analysis commonly takes the form of a power law for comparison with scaling arguments such as those defined by Curle [10] and Lighthill [11] to predict source types. The OASPL and OASPL(A) scale with Mach number, $M^{5.9}$ and $M^{6.3}$, respectively. This suggests low frequency radiation scales closer to the fifth power, and the mid– to high–frequencies scale near the sixth or seventh power. Similar fits have been found; for example, Chong et al. [12] found their levels to scale with $M^{5.3}$ and $M^{6.8}$ at an angle 90° off the jet axis. However, the relative magnitudes of the noise sources can be significantly different among facilities. The OASPL can be used for this discussion, but lacks frequency information and is prone to being largely influenced by only the most dominant source. For these reasons 1/3 octave band SPL is used. Note the A–weighting is kept but does not greatly affect the analysis since each frequency bin is multiplied by the same weighting factor at all flow speeds. Three power fits of the form M^n, varying n, each collapse a part of the spectrum best, as depicted in Figure 6. Below 0.9 kHz, the best fit is found to be $n = 5.3$. The mid–frequency band, 0.9–2.8 kHz, is seen to have a higher power of $n = 7.5$, while beyond 2.8 kHz scales best with $n = 6.8$.

The aforementioned collector treatment can be seen in Fig. 7. The narrow-band SPL spectrum is plotted to allow further investigation of the effects of the Nomex® treatment. A–weighting is not used for the remainder of the figures. Two tunnel speeds are given, but the trends are very similar for

all flow speeds. Below 2 kHz, the two cases are relatively unchanged. However, frequencies beyond 2 kHz show significant attenuation, even reaching 10 dB at 10 kHz.

Two dimensional flow fields are often desired (e.g., for non-swept airfoils) in this facility. For this reason, as well as to reduce acoustic reflections and/or scattering off the model mounting system, thick acoustic foam sidewalls are used. A trade-off exists; they reduce three-dimensional flow effects and minimize acoustic interference from reflections/scattering at the expense of increasing background levels due to sidewall scrubbing noise. Figure 8 shows the difference in background levels with and without acoustic foam sidewalls. The sidewalls shown are for vertically mounted airfoils, allowing the flyover condition to be measured by sideline microphones rather than mounted below the jet. Slight broadband increase is found beyond approximately 2 kHz likely due to sidewall scrubbing noise. It is also interesting to see reduction at lower than approximately 400 Hz. This effect is thought to be due to less allowable divergence of the jet (i.e., shear layer growth) which in turn decreases the amount of turbulence impinging on the jet collector face. It should be noted that smooth metallic hard walls can be used but increase the risk of acoustic standing waves in the test section. However, the proper boundary conditions are largely dependent on the experimental objectives and should be justified accordingly.

It is important to not only have low overall levels, but also an environment that lacks narrow-band spectral features. At tunnel speeds less than 30 m/s, several tones on the order of kHz are present in the SPL spectra. These tones are not directly related to the tunnel speed (i.e., Strouhal scaling) nor do they collapse with Helmholtz scaling, suggesting these are likely mechanical or electrical noise. To locate the tonal origin(s), microphones are placed in several strategic positions around the facility. Two positions will be discussed: one in close proximity to the tunnel drive system, and another outside of the tunnel upstream of the inlet.
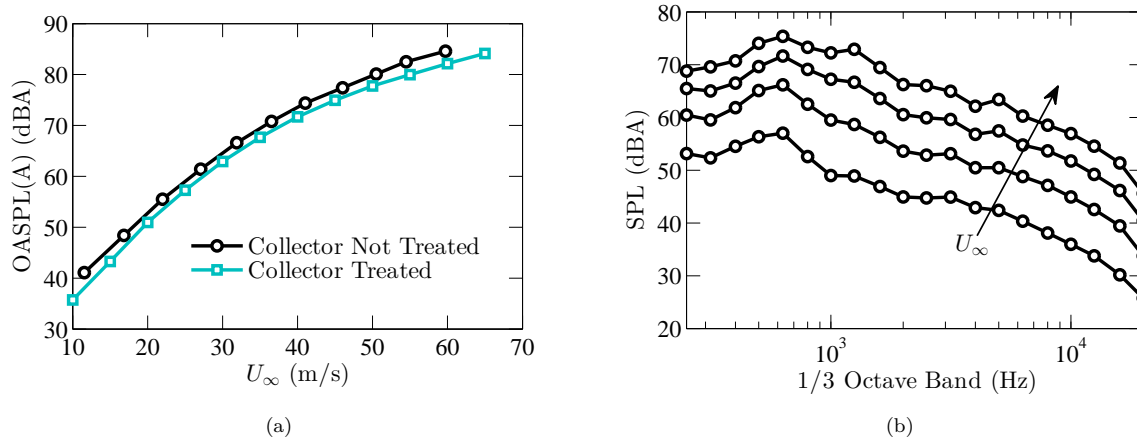

(a)

(b)

Figure 5 – A–weighted background sound levels of sideline measurements for (a) OASPL with and without collector treatment and (b) 1/3 octave bands at tunnel speeds 30-60 m/s, at 10 m/s increments with the collector treated.

The signal acquired near the motor is found to have large amplitude tonal features for all tunnel speeds. These tones are in a harmonic relationship and are unrelated to the blower's blade passage frequency. For this noise to propagate into the test section, one potential propagation path is the upstream inlet. The inlet microphone signal holds much of the same frequency content confirming this situation. To understand the influence of the motor noise on the measurements performed in the test section, the ordinary coherence function [13] is calculated between the signal acquired near the motor, and the microphone signal in the chamber. The result for three tunnel speeds is shown in Fig. 9. At low speeds, high coherence levels are present because all other source levels are relatively small. At 30 m/s, fewer coherence tones exist, but are still identical in frequency to the tones found in Fig. 7(c). Beyond 35 m/s however, background levels exceed motor noise as the coherence holds a near zero value for all frequency bins.

4.3   Expected Upgrades

Although background levels are low enough to obtain a signal-to-noise ratio sufficient for a number of aerodynamic models, this metric can be improved further if handled properly. The discussion in the previous section has given some insight into the major noise sources. Future work will entail
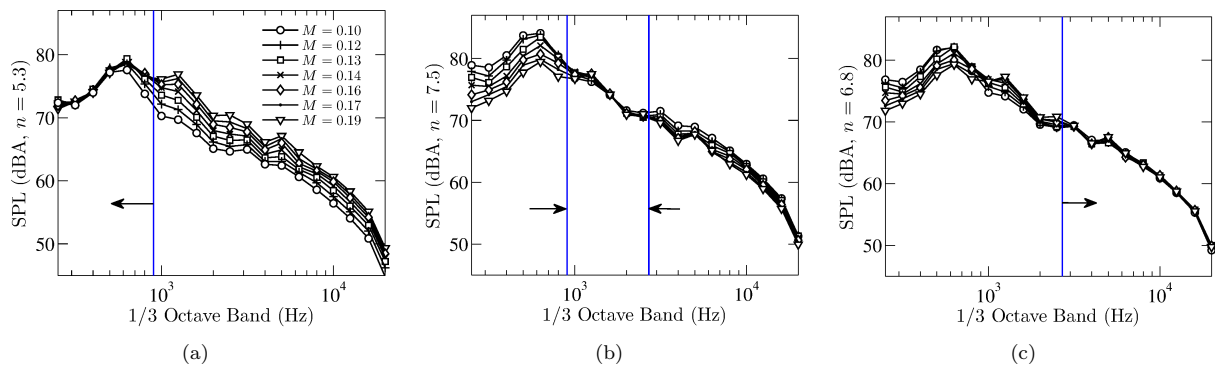
(a)

(b)

(c)

Figure 6 – A–weighted 1/3 octave band SPL of sideline measurements at different freestream Mach numbers, M, scaled with a power law, $\mathrm{SPL} = 10\log_{10}\left(\dfrac{PSD}{P_{ref}^2}\left(\dfrac{M_{ref}}{M}\right)^n\right)$, where $M_{ref} = 0.2$ for (a) $n = 5.3$, (b) $n = 7.5$, and (c) $n = 6.8$. The arrows in each subfigure point out the regions of good collapse.
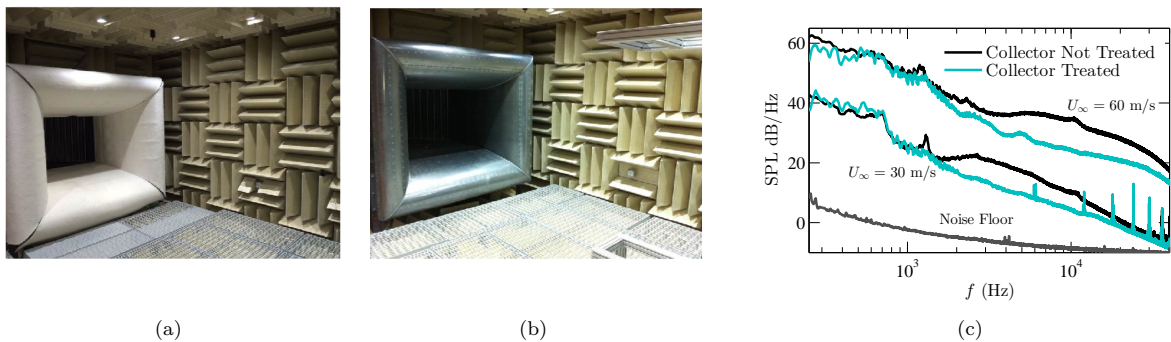

(a)

(b)

(c)

Figure 7 – Images of jet collector looking downstream (a) with and (b) without additional treatment, and (c) the resulting difference in SPL for the sideline microphone 2.3 m from jet, 0.71 m downstream in test section.
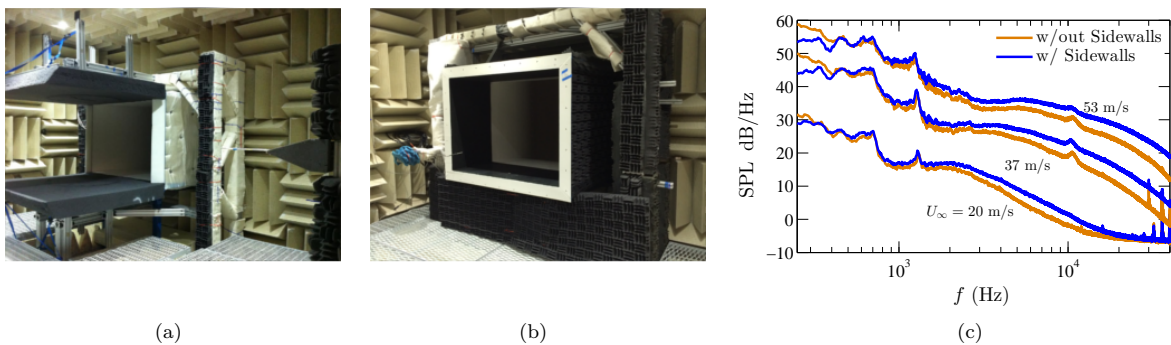

(a)

(b)

(c)

Figure 8 – Images of the inlet looking upstream (a) with and (b) without foam sidewalls, and (c) the resulting difference in SPL for the sideline microphone 2.3 m from jet, 0.71 m downstream in test section.
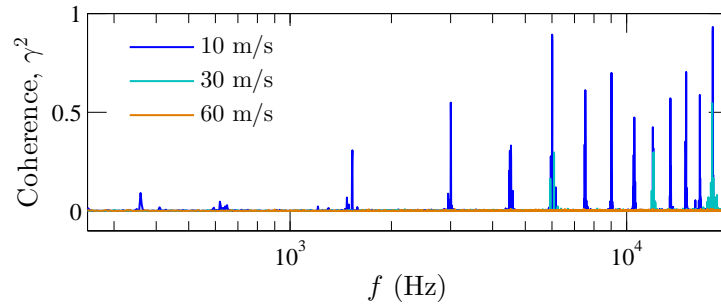
Figure 9 – Coherence between microphone signals acquired near the motor and inside the anechoic chamber.

further investigation of each source, and applying various reduction treatments/techniques. Table 1 summarizes this information along with the expected method of reduction.

Even though overall levels are not affected by the motor, high frequency peaks congest the sound pressure spectrum. An acoustic enclosure surrounding the tunnel motor is proposed to shield upstream tonal propagation, and has been shown to be effective in the facility described by Mathew [4]. The only other mechanical noise known to play a role is generated by the centrifugal blower in the form of low frequency vibrations. Balancing the rotational system will ensure minimal noise impact. Slight improvement is also found via routine greasing of the shaft bearings.

Table 1 – Summary of the dominant noise mechanisms with proposed method of reduction.

Source	Mechanism	Noise Class	Reduction Method
Motor	Mechanical/electrical	> 5 kHz[†]	Acoustic panel housing
Jet collector	Shear layer impingement	< 1 kHz	To be determined
Shear layer	Turbulence	1–3 kHz	To be determined
Turning vanes	Wake impingement, separation	1–10 kHz	Upstream symmetric acoustically treated vanes
Centrifugal blower	Mechanical vibration	< 500 Hz	Balancing, continual greasing of bearings
Sidewalls	Boundary layer scrubbing	1-10 kHz	Investigate other materials, geometry, etc.

[†]Tonal, while others are broadband in the specified frequency range.

Flow noise is the other important source group, and include either impingement on a surface or self-noise due to turbulence. To attenuate wake impingement on the first set of turning vanes, an additional set of symmetric vanes (just upstream) are proposed. Long-chord vanes with acoustic damping characteristics (similar to those in the inlet) will likely be most effective. Geometric parameters such as number of vanes and chord to thickness ratio are yet to be chosen. Although it is likely beneficial to increase the number of vanes, the blockage area ratio must also be considered as this can limit the highest achievable freestream speed.

Sidewall scrubbing noise is due to the interaction of the boundary layer with the coarse surface of the acoustic foam. Investigating the properties of different sidewall configurations (material, characteristic impedance, geometry, etc.) will be useful to establish a baseline reference for designing future experimental setups. The remaining sources are typical issues present in many aeroacoustic tunnels and lack effective treatment techniques. Future work will hopefully progress toward solutions of such problems.

5.　CONCLUSIONS

An overview of the Florida State Aeroacoustic Tunnel has been presented including the several acoustic treatments implemented at the design stage (e.g. inlet silencer, perforate lined ducting,

vibration isolation frames, etc.). The facility's current state is documented in this paper for both flow and acoustic quality. Velocity profiles demonstrate a very uniform jet in the fore region of the test section, and also captures the decay of the potential core with streamwise position. Turbulence intensity is found to be competitive with conventional tunnels in both the open–jet and closed-wall configuration. The anechoic chamber mimics that of a free field for frequencies higher than 250 Hz and is confirmed by comparing with the inverse-square-law. With flow, background levels are competitive, but further reduction below 1 kHz is desired. Above 1 kHz however, reduction is obtained with the additional jet collector treatment. This allows a sufficient signal-to-noise ratio of a model producing peak spectral content in the kHz range, which is typical of this facility given its length scales. The acoustic foam sidewalls are beneficial in many experiments, but increase levels in the mid–frequency range likely being the result of scrubbing noise.

The dominant sources affecting the background noise level have been discussed in detail, along with proposed reduction techniques. Future work will consist of implementing the additional treatment outlined in the previous section.

ACKNOWLEDGMENTS

REFERENCES

1. Leahy J, Lange B. Future Journeys: Global Market Forecast 2013-2032; 2013. [Accessed: 2014 07 23]. Available from: `http://www.airbus.com/company/market/forecast/`.

2. Golub R, Rawls J, Russell J. Evaluation of the Advanced Subsonic Technology Program Noise Reduction Benefits. NASA TM 2005–212144; 2005.

3. Mathew J, Bahr C, Sheplak M, Carroll B, Cattafesta LN. Characterization of an anechoic wind tunnel facility. American Society of Mechanical Engineers; 2005. p. 281–285.

4. Mathew J. Design, fabrication, and characterization of an anechoic wind tunnel facility. PhD Thesis, University of Florida; 2006.

5. Bies DA, Hansen CH. Engineering noise control: theory and practice. CRC Press; 2009.

6. Schlicting H. Boundary-Layer Theory. McGraw-Hill; 1979.

7. Bradshaw P. The understanding and prediction of turbulent flow. Aeronaut J. 1972;76(739):403.

8. Gutmark E, Ho CM. Preferred modes and the spreading rates of jets. Physics of Fluids. 1983;26(10):2932–2938.

9. ISO 3745:2003 Acoustics–Determination of sound power levels of noise sources using sound pressure–Precision methods for anechoic and hemi-anechoic rooms. Geneva, Switzerland; 2003.

10. Curle N. The influence of solid boundaries upon aerodynamic sound. Proceedings of the Royal Society of London Series A Mathematical and Physical Sciences. 1955;231(1187):505–514.

11. Lighthill MJ. On sound generated aerodynamically. I. General theory. Proceedings of the Royal Society of London Series A Mathematical and Physical Sciences. 1952;211(1107):564–587.

12. Chong T, Joseph P, Davies P. Design and performance of an open jet wind tunnel for aero-acoustic measurement. Applied acoustics. 2009;70(4):605–614.

13. Bendat JS, Piersol AG. Random Data: Analysis and Measurement Procedures. Wiley; 2011.